

ELECTRONIC SUPPLEMENTARY INFORMATION

Photoluminescent and Magnetic Properties of Isostructural Europium(III), Gadolinium(III) and Terbium(III) Oxamate-Based Coordination Polymers

Cleverton O. C. da Silveira,^a Willian X. C. Oliveira,^a Eufrânio N. da Silva Júnior,^a Meiry E. Alvarenga,^b Felipe T. Martins,^b Claudia C. Gatto,^c Carlos B. Pinheiro,^d Emerson F. Pedroso,^e Júlia P. O. Silva,^f Lippy F. Marques,^f Moliria V. Santos,^g Francisco R. Torres,^h Rividy Euclides,ⁱ Ricardo O. Freire,ⁱ Wallace C. Nunes,^j Adrielle A. de Almeida,^k Marcelo Knobel^k and Cynthia L. M. Pereira,^{a,*}

^aDepartamento de Química, Instituto de Ciências Exatas, Universidade Federal de Minas Gerais.
Av. Antônio Carlos 6627, Pampulha, Belo Horizonte, Minas Gerais, 31270-901 Brazil. e-mail:
cynthialopes@ufmg.br;

^bInstituto de Química, Universidade Federal de Goiás, Campus Samambaia
Setor Itatiaia, Caixa Postal 131, Goiânia, Goiás, 74001970, Brazil;

^cInstituto de Química, Universidade de Brasília, Asa Norte, Brasília, Distrito Federal, 70904970,
Brazil;

^dDepartamento de Física, Instituto de Ciências Exatas, Universidade Federal de Minas Gerais.
Av. Antônio Carlos 6627, Pampulha, Belo Horizonte, Minas Gerais, 31270-901 Brazil;

^eDepartamento de Química, Centro Federal de Educação Tecnológica de Minas Gerais, Av.
Amazonas, 5253, Belo Horizonte, MG, 30421-169, Brazil;

^fGrupo de Química de Coordenação e Espectroscopia de Lantanídeos (GQCEL), Universidade
do Estado do Rio de Janeiro, Centro de Tecnologia de Ciências, Instituto de Química,
Maracanã, Rio de Janeiro, 20550-900, Brazil;

^gBiosmart Nanotechnology Ltda, Avenida Jorge Fernandes de São Mattos, 311, box 4,
Araraquara, 14808-162, SP, Brazil;

^hDepartamento de Química, Faculdade de Filosofia, Ciências e Letras de Ribeirão Preto,
Universidade de São Paulo, 14040901 - Ribeirão Preto, SP, Brazil;

ⁱPople Computational Chemistry Laboratory, Departamento de Química, Universidade Federal de Sergipe, São Cristóvão-SE, 49100-000, Brazil;

^jInstituto de Física, Universidade Federal Fluminense, Av. Gal. Milton Tavares de Souza, s/nº, Niterói 24210-346, RJ, Brazil;

^kInstituto de Física Gleb Wataghin, Universidade Estadual de Campinas, Rua Sérgio Buarque de Holanda, 777, Cidade Universitária Zeferino Vaz, Barão Geraldo, Campinas, SP, 13083-859, Brazil.

1. Experimental details of solid-state photophysical studies

1.1. Experimental photophysical studies

Experimental intensity parameters, Ω_λ , for the Eu³⁺ coordination polymer was determined from the emission spectra using the following Eq. 1:^{1,2}

$$\Omega_\lambda = \frac{3\hbar c^3 A_{0 \rightarrow J}}{4e^2 \omega^3 \chi \left\langle {}^7F_J \left\| U^{(\lambda)} \right\| {}^5D_0 \right\rangle^2} \quad (1)$$

where χ is the Lorentz local field correction term, given by $\chi = n(n+2)^2/9$ and $\left\langle {}^7F_J \left\| U^{(\lambda)} \right\| {}^5D_0 \right\rangle^2$ is a squared reduced matrix element with value of 0.0032 for the ${}^5D_0 \rightarrow {}^7F_2$ transition and 0.0023 for the ${}^5D_0 \rightarrow {}^7F_4$ one. The refractive index (n) has been assumed equal to 1.5. In this work, the ${}^5D_0 \rightarrow {}^7F_6$ transition was not observed experimentally; thus, the experimental Ω_6 parameter could not be estimated. The spontaneous emission coefficient, $A_{01} = 0.31 \times 10^{-11}(n)^3(v_{01})^3$, leading to an estimated value around 50 s^{-1} for the refractive index (n) defined above. In Eq. (1), the $A_{0\lambda}$ term, where $\lambda = 2$ and 4, represents the spontaneous emission coefficients of the ${}^5D_0 \rightarrow {}^7F_2$ and ${}^5D_0 \rightarrow {}^7F_4$ transitions, which can be calculated from ${}^5D_0 \rightarrow {}^7F_1$ reference transition (magnetic dipole mechanism), therefore this transition is practically insensitive to chemical environment changing, Eq. (2).

$$A_{0\lambda} = \frac{v_{01}}{v_{0\lambda}} \frac{S_{0\lambda}}{S_{01}} (A_{01}) \quad (2)$$

Where S_{01} and $S_{0\lambda}$ are the areas under the curves of the ${}^5D_0 \rightarrow {}^7F_1$ and ${}^5D_0 \rightarrow {}^7F_\lambda$ transitions, with v_{01} and $v_{0\lambda}$ being their energy barycenters respectively.

1.2. Theoretical calculations

The luminescent properties were calculated using the LUMPAC program.³ Initially, the Judd-Ofelt theory was used to calculate the intensity parameters Ω_λ ($\lambda = 2$, 4, and 6) (Eq (3)).^{4,5}

$$\Omega_\lambda = (2\lambda+1) \sum_{t=\lambda-1}^{\lambda+1(odd)} \sum_{p=-t}^{t(all)} \frac{|B_{\lambda tp}|^2}{(2t+1)} \quad (3)$$

Where the $B_{\lambda tp}$ term is the sum of the forced electric dipole (ed) dynamics coupling (dc) contributions (Eq. (4)):

$$B_{\lambda tp} = \frac{2}{\Delta E} \langle r^{t+1} \rangle \theta(t, \lambda) \gamma_p^t + \left(- \left[\frac{(\lambda+1)(2\lambda+3)}{2\lambda+1} \right]^{\frac{1}{2}} \langle r^\lambda \rangle (1-\sigma_\lambda) \langle f \| C^{(\lambda)} \| f \rangle \Gamma_p^t \delta_{t,\lambda+1} \right) \quad (4)$$

All the terms appearing in this equation are thoroughly explained in the reference⁶ and in the LUMPAC homepage (<https://www.lumpac.pro.br/theory>).

The calculation of intensity parameters depends on the charge factors and polarizabilities associated with the bonds between the Eu³⁺ ion and the ligand atoms. Since there are no analytical equations for calculating these quantities, we proceed with their adjustment using the QDC model,⁷ aiming to fit the calculated Ω_2 and Ω_4 parameters to their respective experimental values.

From the calculated intensity parameters, it was possible to calculate the energy transfer and back transfer rates using the model developed by Malta and coworkers.⁸ According to this model, the energy transfer rates, WET, can be determined from the sum of two terms (Eq. (5)):

$$W_{ET} = W_{ET}^{mm} + W_{ET}^{em} \quad (5)$$

The W_{ET}^{mm} term corresponds to the energy transfer rate obtained from the multipolar mechanism (Eq. (6)):

$$W_{ET}^{mm} = \frac{2\pi}{\hbar} = \frac{e^2 S_L}{(2J+1)G} F \sum_\lambda \gamma_\lambda \langle \alpha' J' \| U^{(\lambda)} \| \alpha J \rangle^2 + \frac{4\pi}{\hbar} \frac{e^2 S_L}{(2J+1)GR_L^6} F \sum_\lambda \Omega_\lambda^{ed} \langle \alpha' J' \| U^{(\lambda)} \| \alpha J \rangle^2 \quad (6)$$

and the W_{ET}^{em} term refers to the energy transfer rates obtained from the exchange mechanism (Eq. (7)):

$$W_{ET}^{em} = \frac{8\pi}{3\hbar} \frac{e^2 (1-\sigma_0)^2}{(2J+1)R_L^4} F \langle \alpha' J' \| S \| \alpha J \rangle^2 \sum_m \left| \left\langle \varphi \left| \sum_k \mu_z(k) s_m(k) \right| \varphi' \right\rangle \right|^2 \quad (7)$$

All the terms appearing in this equation are thoroughly explained in the reference⁶ and in the LUMPAC homepage (<https://www.lumpac.pro.br/theory>).

$$A\left({}^5D_0 - {}^7F_J\right) = \frac{64\pi^4 v^3}{3h(2J+1)} \left[\frac{n(n^2+2)^2}{9} S_{ed} + n^3 S_{md} \right] \quad (8)$$

The intensity parameters were also used to determine the radiative emission rate (A_{rad}). The non-radiative emission rate (A_{nrad}) was calculated from A_{rad} according to Equation (9).

$$\frac{1}{\tau} = A_{rad} + A_{nrad} \quad (9)$$

The energy transfer and back transfer rates, along with the rates of radiative and non-radiative emission, made it possible to calculate, from Equations (10) and (11), the quantum efficiency (η) and the quantum yield (q).

$$\eta = \frac{A_{rad}}{A_{rad} + A_{nrad}} \quad (10)$$

$$q = \frac{A_{rad}\eta_{{}^5D_0}}{\varphi\eta_{S_0}} \quad (11)$$

where $\eta_{{}^5D_0}$ is the 5D_0 level population. and η_{S_0} correspond to the S_0 singlet level population and absorption rate, respectively.

2. Figures

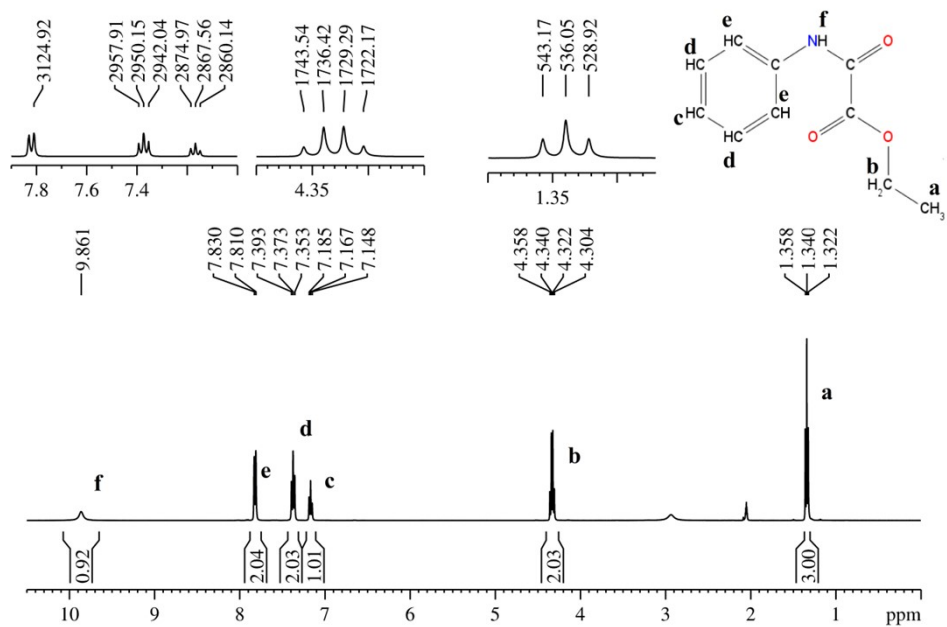


Fig. S1 ¹H NMR spectrum for Etphox in $(CD_3)_2CO$ (400 MHz, r. t.).

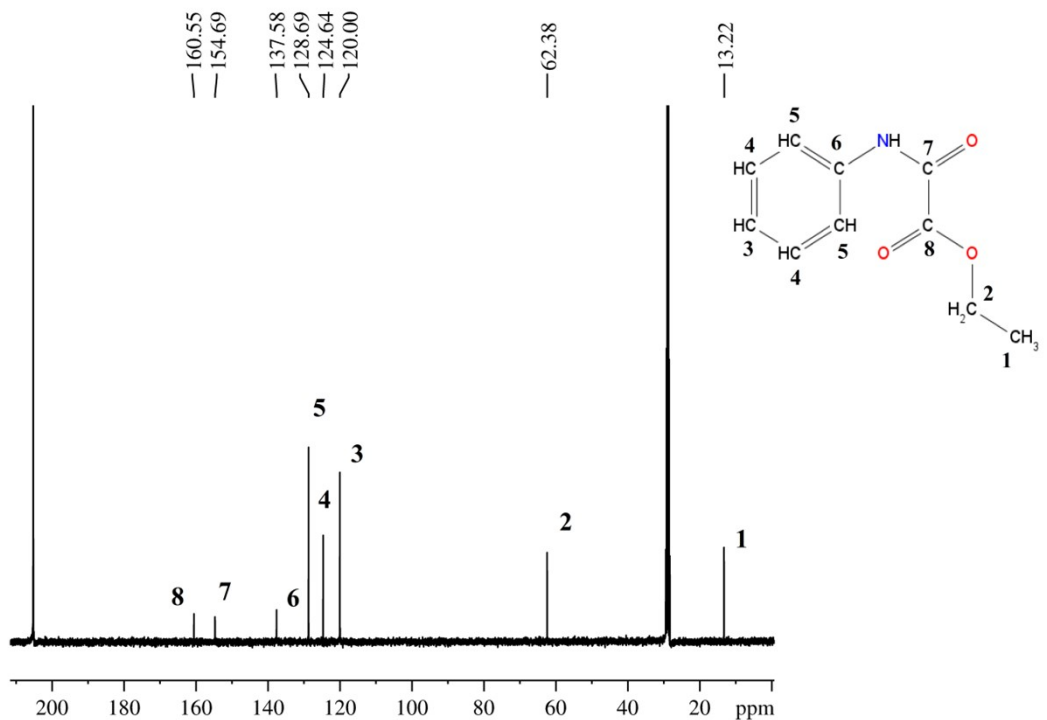


Fig. S2 ¹³C NMR spectrum for Etphox in $(CD_3)_2CO$ (101 MHz, r. t.)

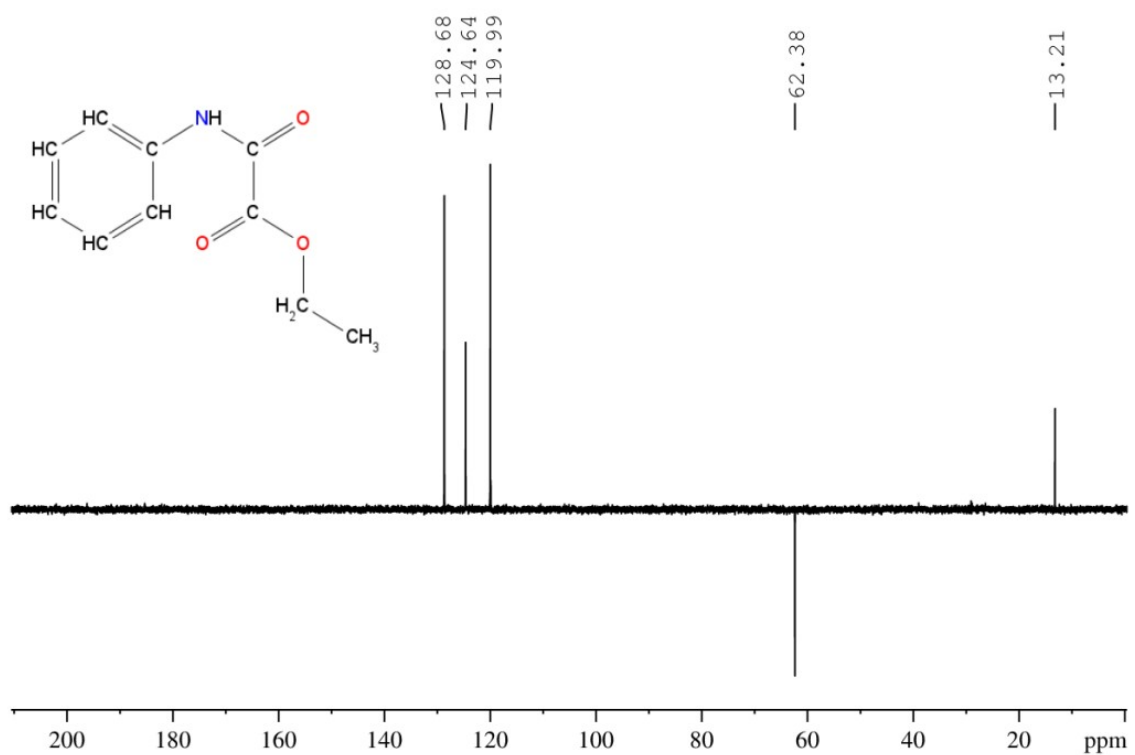


Fig. S3 ^{13}C DEPT-135 spectrum for Etphox in $(\text{CD}_3)_2\text{CO}$ (101 MHz, r. t.).

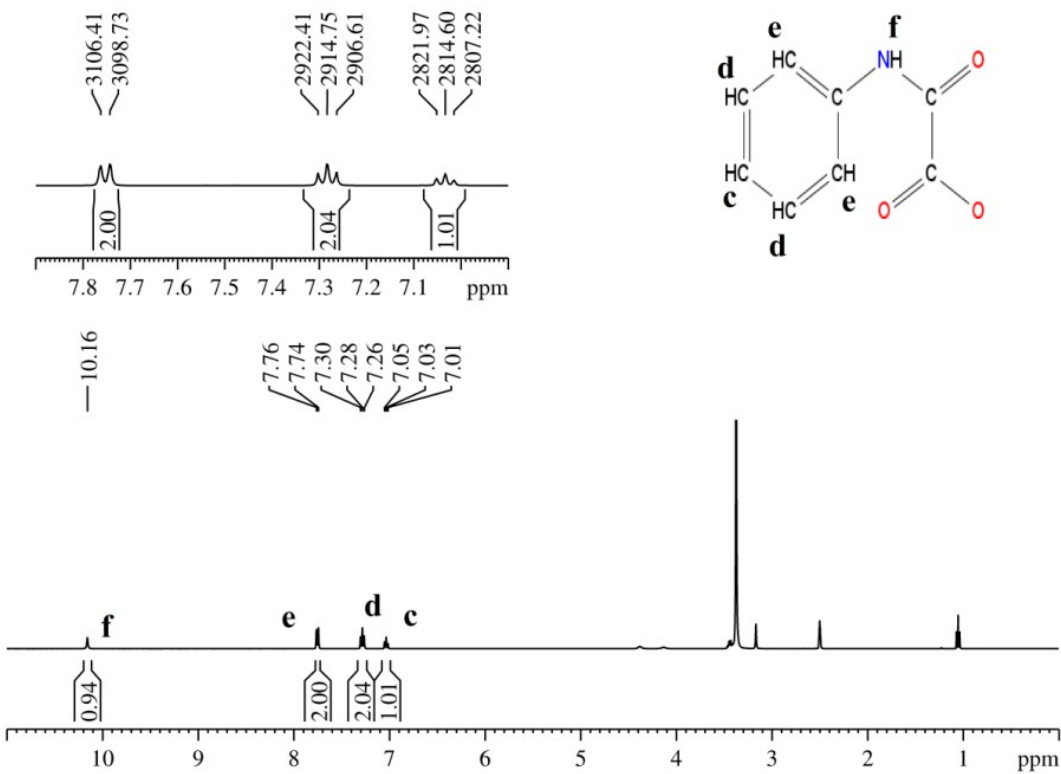


Fig. S4 ^1H NMR spectrum for Naphox in $(\text{CD}_3)_2\text{SO}$ (400 MHz, r. t.).

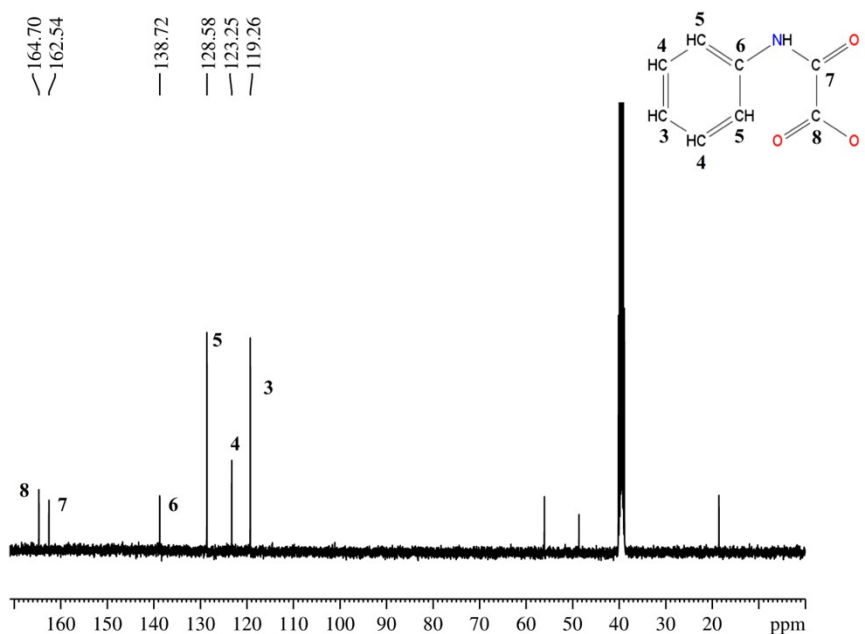


Fig. S5 ^{13}C NMR spectrum for Etphox in $(\text{CD}_3)_2\text{CO}$ (101 MHz, r. t.).

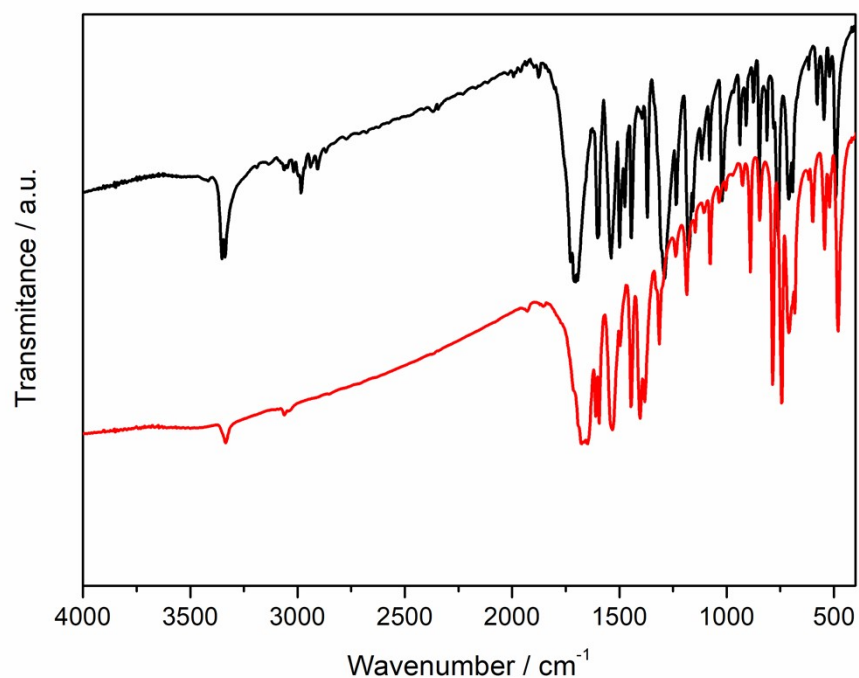


Fig. S6 IR spectra of Etphox (black line) and Naphox (red line).

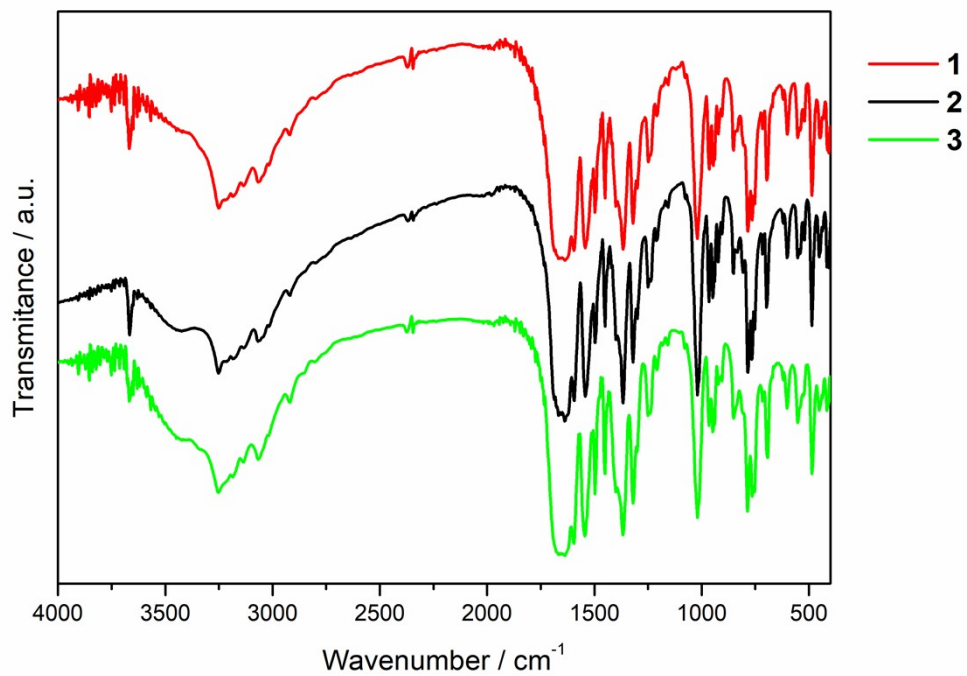


Fig. S7 IR data of **1**, **2** and **3**.

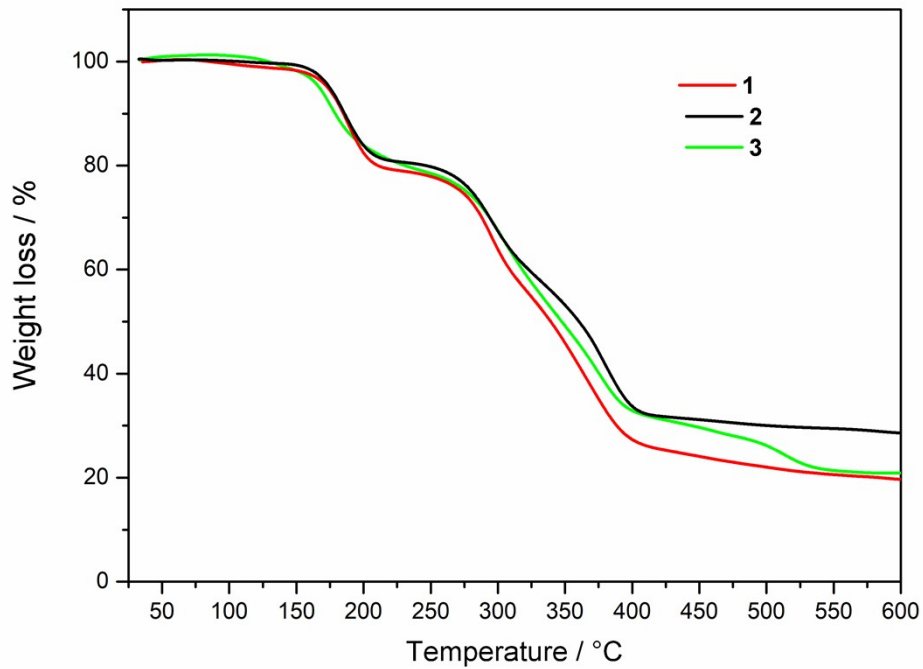


Fig. S8 TG curves of **1**, **2** and **3**.

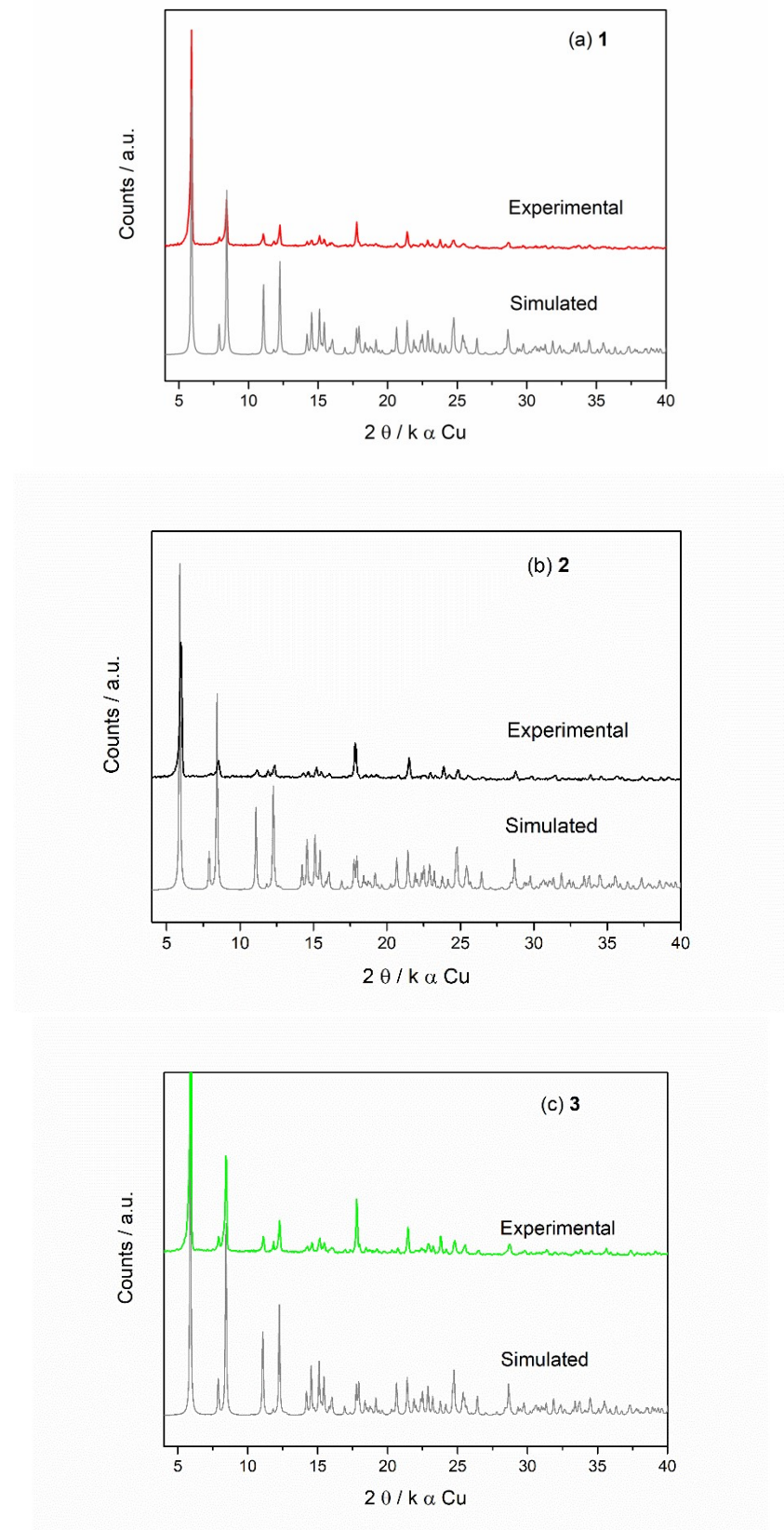


Fig. S9 Experimental and simulated X-ray diffraction patterns of (a) **1**, (b) **2** and (c) **3**.

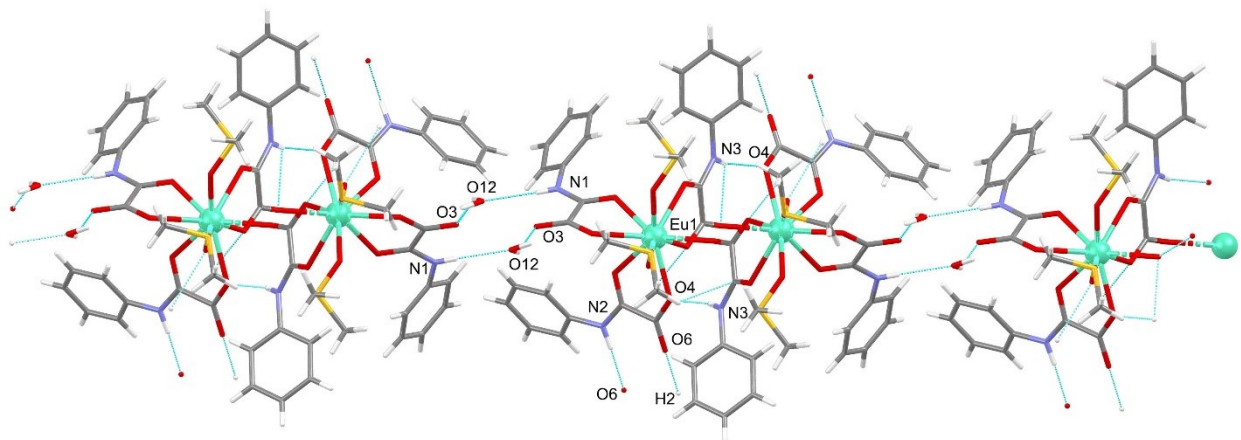


Fig. S10 Representation of the one-dimensional network of **1** by hydrogen bonds view through the [010] direction. Interactions are represented by cyan dashed lines.

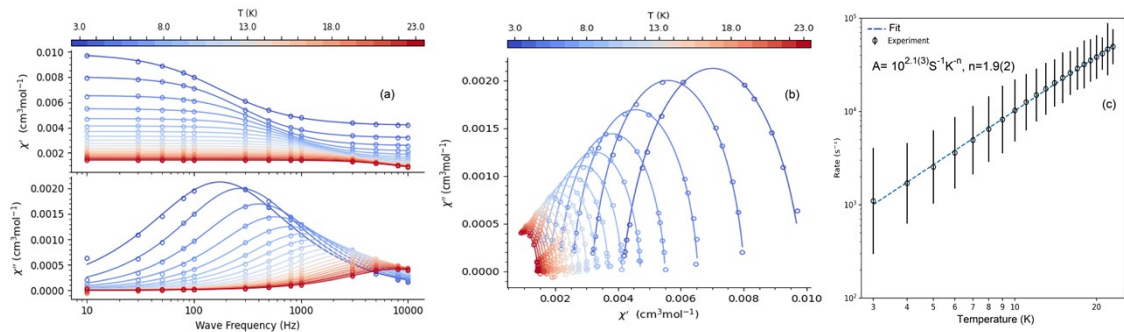


Fig. S11 Ac susceptibility data for **2**. (a) Frequency dependence of the in-phase (χ') and out-of-phase (χ'') components of the ac magnetic susceptibility taken at various temperatures using a dc magnetic field of 1 kOe; solid lines correspond to the fit using the generalized Debye model. (b) Cole-Cole plot using the dc magnetic field of 1 kOe with solid lines corresponding to the generalized Debye model fitting results. (c) Temperature dependence of the relaxation time and their fit using the phonon bottleneck effect.

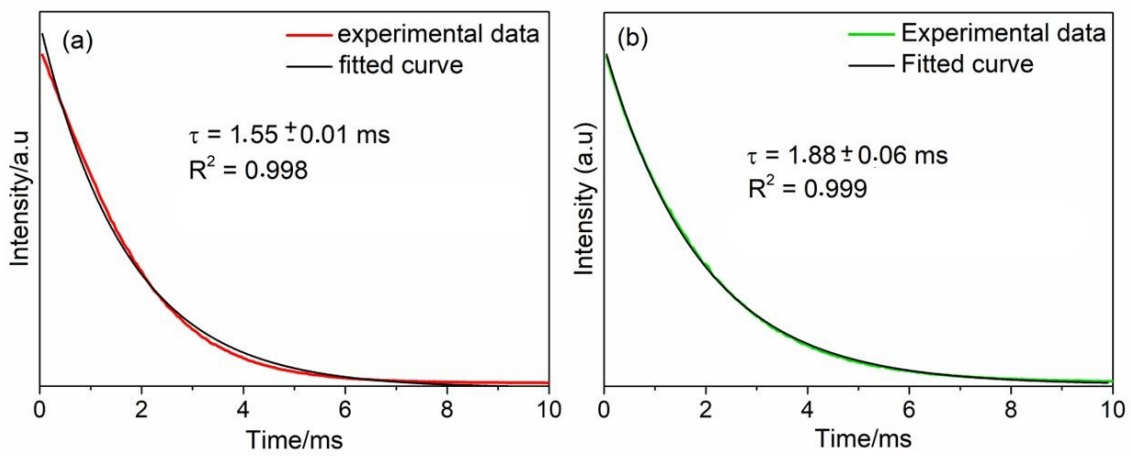


Fig. S12 Lifetime decay for (a) **1** and (b) **3**, under excitation at 275.2 nm and 276.2 nm, respectively.

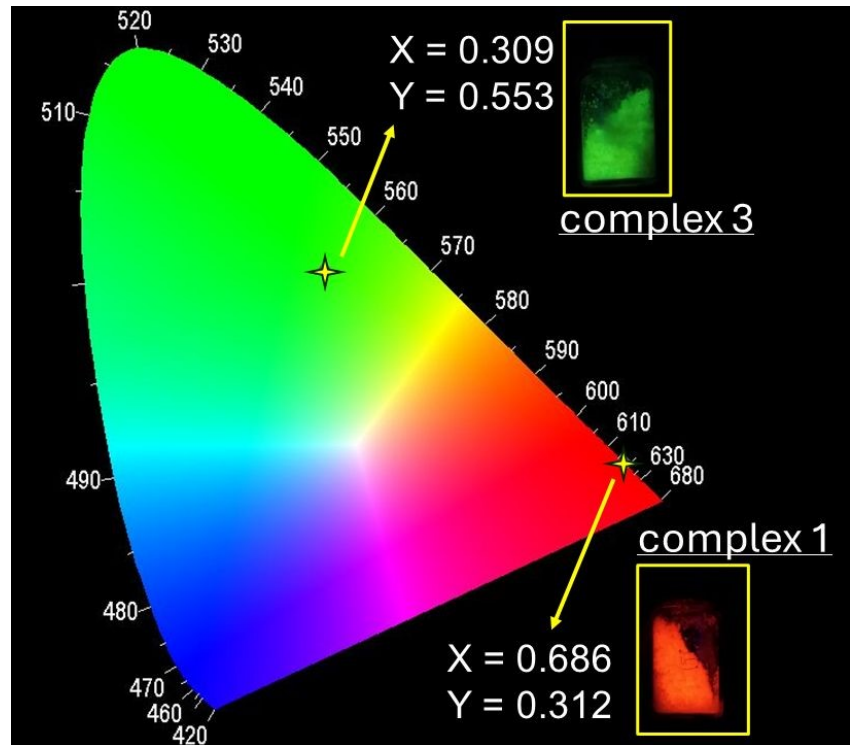


Fig. S13 Chromaticity diagram obtained from the emission spectra of the **1** and **3** oxamate complexes. The inserts display photographs of complexes **1** and **3** obtained with a digital camera indicating the intense photoluminescence in the red region observed under UV irradiation.

3. Tables

Table S1. Selected bond lengths (\AA) and angles ($^\circ$) for **1**.

Bond lengths (\AA)		Bond angles ($^\circ$)	
Eu(1)–O(1)	2.423(6)	O(1)–Eu(1)–O(9) ⁱ	141.3(2)
Eu(1)–O(2)	2.522(6)	O(10)–Eu(1)–O(9) ⁱ	73.86(19)
Eu(1)–O(4)	2.460(6)	O(1)–Eu(1)–O(4)	107.3(2)
Eu(1)–O(5)	2.488(5)	O(4)–Eu(1)–O(7)	70.81(19)
Eu(1)–O(7)	2.487(6)	O(4)–Eu(1)–O(5)	64.57(19)
Eu(1)–O(8)	2.507(5)	O(10)–Eu(1)–O(8)	138.72(18)
Eu(1)–O(9) ⁱ	2.460(6)	O(11)–Eu(1)–O(7)	134.17(19)
Eu(1)–O(10)	2.436(6)	O(11)–Eu(1)–O(10)	74.7(2)
Eu(1)–O(11)	2.378(6)	O(11)–Eu(1)–O(1)	75.8(2)

Symmetry operations (ⁱ) = $-x+3/2, y-1/2, -z+3/2$.

Table S2. Selected bond lengths (\AA) and angles ($^\circ$) for **2**.

Bond lengths (\AA)	Bond angles ($^\circ$)
Gd1–O2	O2–Gd1–O3 64.65 (8)
Gd1–O3	O2–Gd1–O4 75.17 (8)
Gd1–O4	O2–Gd1–O5i 70.35 (8)
Gd1–O5i	O2–Gd1–O6 128.64 (8)
Gd1–O6	O2–Gd1–O7 107.51 (9)
Gd1–O7	O2–Gd1–O9 131.65 (8)
Gd1–O9	O2–Gd1–O10 140.76 (9)
Gd1–O10	O2–Gd1–O11 69.47 (8)
Gd1–O11	O4–Gd1–O3 137.74 (8)
	O3–Gd1–O5i 73.21 (8)
	O3–Gd1–O6 118.85 (8)
	O3–Gd1–O7 68.03 (9)
	O3–Gd1–O9 68.99 (9)
	O3–Gd1–O10 141.71 (9)
	O3–Gd1–O11 102.33 (9)
	O4–Gd1–O5i 81.75 (8)
	O4–Gd1–O6 76.64 (8)
	O4–Gd1–O7 140.73 (9)
	O4–Gd1–O9 142.02 (8)
	O4–Gd1–O10 79.23 (9)
	O4–Gd1–O11 73.83 (8)
	O5i–Gd1–O6 63.76 (7)
	O5i–Gd1–O7 136.93 (9)
	O5i–Gd1–O9 84.16 (9)
	O5i–Gd1–O10 134.31 (8)
	O5i–Gd1–O11 136.99 (9)
	O7–Gd1–O6 121.38 (9)
	O6–Gd1–O9 65.49 (8)
	O6–Gd1–O10 71.56 (8)
	O6–Gd1–O11 138.79 (8)
	O7–Gd1–O9 65.17 (9)
	O7–Gd1–O10 75.39 (10)
	O7–Gd1–O11 71.02 (9)
	O9–Gd1–O10 85.98 (10)
	O9–Gd1–O11 135.40 (9)
	O10–Gd1–O11 75.16 (9)

Symmetry operations (i) = $-x+3/2, y-1/2, -z+1/2$.

Table S3. Selected bond lengths (\AA) and angles ($^\circ$) for **3**.

Bond lengths (\AA)		Bond angles ($^\circ$)	
Tb(01)–O(1)	2.450(3)	O(1)–Eu(1)–O(9) ⁱ	70.55(11)
Tb(01)–O(2)	2.494(3)	O(10)–Eu(1)–O(9) ⁱ	134.27(12)
Tb(01)–O(4)	2.416(4)	O(1)–Eu(1)–O(4)	107.43(12)
Tb(01)–O(5)	2.533(3)	O(4)–Eu(1)–O(7)	140.89(12)
Tb(01)–O(7)	2.454(3)	O(4)–Eu(1)–O(5)	64.86(12)
Tb(01)–O(8) ⁱ	2.504(3)	O(10)–Eu(1)–O(8)	71.55(11)
Tb(01)–O(9) ⁱ	2.498(3)	O(11)–Eu(1)–O(7)	73.75(11)
Tb(01)–O(10)	2.381(3)	O(11)–Eu(1)–O(10)	74.81(2)
Tb(01)–O(11)	2.436(3)	O(11)–Eu(1)–O(1)	69.56(11)

Symmetry operations (ⁱ) = $-x+I/2, y+I/2, -z+I/2$.

Table S4. CShM calculations of the coordination environment at metal(III) ion in all complexes of ML_9 coordination sphere.^a

Compound	EP-9	OPY-9	HBPY-9	JTC-9	JCCU-9	CCU-9	JCSAPR-9	CSAPR-9	JTCTPR-9	TCTPR-9	JTDIC-9	HH-9	MFF-9
1	37.134	22.108	18.815	15.670	11.117	9.647	1.523	0.398	3.038	1.234	12.591	11.417	0.453
2	37.154	22.081	18.912	15.760	11.079	9.599	1.519	0.381	3.025	1.207	12.689	11.361	0.453
3	37.173	22.054	18.903	15.690	11.093	9.600	1.544	0.393	3.070	1.225	12.617	11.400	0.455

^aAbbreviations: EP-9 = Enneagon (D_{9h}); OPY-9= Octagonal pyramid (C_{8v}); HBPY-9 = Heptagonal bipyramid (D_{7h}); JTC-9 = Johnson triangular cupola J3 (C_{3v}); JCCU-9 = Capped cube J8 (C_{4v}); CCU-9 = Spherical-relaxed capped cube (C_{4v}); JCSAPR-9 = Capped square antiprism J10 (C_{4v}); CSAPR-9 = Spherical capped square antiprism (C_{4v}); JTCTPR-9 = Tricapped trigonal prism J51 (D_{3h}); TCTPR-9 = Spherical tricapped trigonal prism (D_{3h}); JTDIC-9 = Tridiminished icosahedron J63 (C_{3v}); HH-9 = Hula-hoop (C_{2v}); MFF-9 = Muffin (C_s)

Table S5. Debye parameters from the AC susceptibility data were measured with an applied magnetic field of 1 kOe for **2**.

T / K	τ / s	χ_T / $\text{cm}^3 \text{ mol}^{-1} \text{ K}$	χ_s / $\text{cm}^3 \text{ mol}^{-1} \text{ K}$	α
3	9.10E-4	0.001194	0.009895	0.19
4	5.88E-4	0.003171	0.008031	0.12
5	3.93E-4	0.002549	0.006551	0.11
6	2.77E-4	0.002123	0.005503	0.10
7	2.03E-4	0.001820	0.004719	0.09
8	1.54E-4	0.001592	0.004132	0.09
9	1.22E-4	0.001407	0.003699	0.09
10	9.74E-5	0.001273	0.003315	0.08
11	7.95E-5	0.001163	0.003003	0.07
12	6.66E-5	0.001069	0.002751	0.06
13	5.70E-5	9.890E-04	0.002541	0.06
14	4.95E-5	9.199E-04	0.002363	0.05
15	4.35E-5	8.562E-04	0.002209	0.05
16	3.86E-5	8.104E-04	0.002064	0.04
17	3.46E-5	7.660E-04	0.001938	0.04
18	3.13E-5	7.222E-04	0.001833	0.04
19	2.84E-5	6.815E-04	0.001738	0.04
20	2.61E-5	6.586E-04	0.001647	0.03
21	2.38E-5	6.199E-04	0.001572	0.03
22	2.18E-5	5.910E-04	0.001498	0.03
23	2.02E-5	5.677E-04	0.001431	0.03

Table S6. Debye parameters from the AC susceptibility data were measured with an applied magnetic field of 2.5 kOe for **2**.

T / K	τ / s	χ_T / cm ³ mol ⁻¹ K	χ_s / cm ³ mol ⁻¹ K	α
3	0.001658	3.43E-4	0.002614	0.27
4	0.001244	2.9E-4	0.002753	0.15
5	8.848E-04	2.4E-4	0.002476	0.11
6	6.258E-04	2.02E-4	0.002148	0.10
7	4.535E-04	1.74E-4	0.001870	0.09
8	3.372E-04	1.5E-4	0.001650	0.08
9	2.573E-04	1.34E-4	0.001464	0.07
10	2.024E-04	1.20E-4	0.001324	0.07
11	1.613E-04	1.10E-4	0.001198	0.06
12	1.322E-04	1.01E-4	0.001101	0.06
13	1.100E-04	9.35E-5	0.001016	0.05
14	9.286E-05	8.76E-5	9.418E-04	0.04
15	7.983E-05	8.26E-5	8.804E-04	0.04
16	6.943E-05	7.82E-5	8.249E-04	0.04
17	6.090E-05	7.41E-5	7.742E-04	0.03
18	5.452E-05	6.93E-5	7.346E-04	0.04
19	4.903E-05	6.66E-5	6.976E-04	0.04
20	4.422E-05	6.26E-5	6.643E-04	0.04
21	3.995E-05	6.10E-5	6.292E-04	0.03
22	3.640E-05	5.91E-5	5.993E-04	0.03
23	3.340E-05	5.68E-5	5.739E-04	0.02
24	3.069E-05	5.42E-5	5.500E-04	0.02
25	2.825E-05	5.31E-5	5.258E-04	0.02
26	2.618E-05	5.21E-5	5.053E-04	0.02
27	2.428E-05	5.39E-5	4.820E-04	0.01
28	2.274E-05	5.07E-5	4.684E-04	0.01
29	2.109E-05	4.45E-5	4.558E-04	0.02
30	1.965E-05	4.38E-5	4.388E-04	0.02
31	1.834E-05	4.16E-5	4.246E-04	0.02
32	1.719E-05	4.01E-5	4.113E-04	0.02
33	1.615E-05	3.99E-5	3.976E-04	0.01

Table S7. Spherical Atomic Coordinates for the Sparkle/PM3 model Coordination Polyhedron, Charge Factors (g), and the Polarizability (α) of the Coordinated Ligating Atoms for **1**.

Atom	R (Å)	Θ (°)	Φ (°)	g	α (Å ³)
Eu	0.0000	0.00	0.00	-	-
O	2.4534	79.09	73.09	0.2396	6.1792
O	2.4975	94.28	358.46	0.2434	3.3989
O	2.4813	21.75	337.99	0.2433	3.9535
O	2.4902	134.72	240.74	0.2435	4.2736
O	2.5123	88.41	301.34	0.2361	4.7835
O	2.5131	34.88	153.63	0.2372	5.5842
O	2.5104	80.11	222.36	0.2366	5.1597
O	2.4430	153.51	49.21	0.2479	3.6369
O	2.4358	106.83	143.58	0.2477	3.7028

References

- ¹ W. T. Carnall, H. M. Crosswhite, "Energy Structure and Transitions Probabilities in LnF_3 of the Trivalent Lanthanides", Argonne National Laboratory Report, Argonne, IL, 1977.
- ² R. Pavithran, N. S. S. Kumar, S. Biju, M. L. P. Reddy, S.A. Júnior, R. O. Freire, *Inorg. Chem.* 45 (2006) p. 2184 – 2192.
- ³ J. D. L. Dutra, T. D. Bispo, R. O. Freire, *J. Comput. Chem.* 35 (2014) p. 772 – 775.
- ⁴ B. R. Judd, *Phys. Rev.* 127 (1962) 750 – 761.
- ⁵ G. S. Ofelt, *J. Chem. Phys.* 37 (1962) 511 – 520.
- ⁶ E. M. Gomes, D. F. Franco, S. L. Scarpari, M. V. Colaço, M. S. Ferreira, R. O. Freire, L. F., *J. Lumin.* 210 (2019) p. 104 – 118.
- ⁷ J.D.L. Dutra, N.B.D. Lima, R.O. Freire, A.M. Simas, *Sci. Rep.* 5 (2015), 13695.
- ⁸ Carneiro Neto, A. N.; Teotonio, E. E. S.; de Sa, G. F.; Brito, H. F.; Legendziewicz, J.; Carlos, L. D.; Felinto, M. C. F. C.; Gawryszewska, P.; Moura Jr, R. T.; Longo, R. L.; Faustino, W. M.; Malta, O. L. Modeling intramolecular energy transfer in lanthanide chelates: A critical review and recent advances. Chapter 310 - Modeling intramolecular energy transfer in lanthanide chelates: A critical review and recent advances, in Handbook on the Physics and Chemistry of Rare Earths, J.-C. G. Bunzli and V. K. Pecharsky, Editors. 2019, Elsevier. p. 55-162.
doi:10.1016/bs.hpcr.2019.08.001.